

## High-resolution climate projections for the islands of Lombok and Sumbawa, Nusa Tenggara Barat Province, Indonesia: Challenges and implications<sup>☆</sup>



John L. McGregor\*, Kim C. Nguyen, Dewi G.C. Kirono, Jack J. Katzfey

Oceans and Atmosphere Flagship, Commonwealth Scientific and Industrial Research Organization (CSIRO), Private Bag No. 1, Aspendale, Victoria 3195, Australia

### ARTICLE INFO

#### Article history:

Available online 11 November 2015

#### Keywords:

Regional climate modelling  
Downscaling  
Fine resolution

### ABSTRACT

The regional climate of Nusa Tenggara Barat (NTB) Province, eastern Indonesia is simulated for 130 years (1971–2100) for the SRES A2 Delayed Development or ‘Business as Usual’ emissions scenario using the CSIRO conformal-cubic atmospheric model (CCAM). Regional climate simulations are generated using a multiple downscaling technique where a CCAM 200 km uniform-grid global simulation is driven by bias-corrected sea surface temperatures (SSTs) from host coupled Global Climate Models (GCMs). Next, the 200 km resolution CCAM simulations are dynamically downscaled to 14 km resolution for the islands of Lombok and Sumbawa. To provide an ensemble of results, separate simulations are performed from six host GCMs. The present-day model results are validated against available observations. Generally, the CCAM 14 km resolution simulations produce rainfall, maximum and minimum temperatures that are similar to the observations. However, the 14 km simulations have rainfall biases of around 5 mm/day in the wet December–February season and lesser biases in the other seasons. Climate projections are examined for two future time intervals centred on 2030 and 2060. The simulations of rainfall changes by 2060 suggest both increases and decreases of up to 5% in December–February, with more acute declines of 10% in some areas, and decreases of up to 10% in March–May. For the other seasons, generally little change is simulated. The regional temperatures are projected to increase by about 1 °C by 2030 and 1.6–2 °C by 2060. The high-resolution model outputs enable detailed differentiation between locations across the islands. Our results show that due to orographic effects there are steep climate gradients, resulting in significant local differences in climate projections. We discuss the challenges and implications of these results for adaptation planning.

© 2015 The Authors. Published by Elsevier B.V. This is an open access article under the CC BY-NC-ND license (<http://creativecommons.org/licenses/by-nc-nd/4.0/>).

### Introduction

The climate of Indonesia's eastern island archipelago is highly variable, both temporally and spatially. The climate is strongly influenced by monsoon and trade winds which are responsible for the two distinct seasons experienced across

\* A paper for submission to Climate Risk Management, Special Edition on Bridging scales and knowledge cultures for adaptation pathways in eastern Indonesia: an integrated approach, 31 March 2015.

\* Corresponding author.

E-mail addresses: [John.McGregor@csiro.au](mailto:John.McGregor@csiro.au) (J.L. McGregor), [Kim.C.Nguyen@csiro.au](mailto:Kim.C.Nguyen@csiro.au) (K.C. Nguyen), [Dewi.Kirono@csiro.au](mailto:Dewi.Kirono@csiro.au) (D.G.C. Kirono), [Jack.Katzfey@csiro.au](mailto:Jack.Katzfey@csiro.au) (J.J. Katzfey).

the entire Indonesian archipelago. The NTB dry season (April–October) occurs as a result of the dry south-easterly trade winds, while the wet season (November–March) occurs when the monsoon winds blow from a north-westerly direction, carrying air masses from mainland Asia and the Indo-west Pacific Ocean. As described further by [Kirono et al. \(2016\)](#), orographic effects on rainfall are also apparent across the NTB islands.

Temporally, there is significant interannual variability in seasonal rainfall over the Indonesian archipelago, which is closely related to large-scale ocean–atmosphere phenomena such as the El Niño Southern Oscillation (ENSO). Over the NTB, the interannual variability is particularly apparent for the dry season; this is discussed in detail by [Kirono et al. \(2016\)](#). There is already evidence of climate change over Indonesia. [Hulme and Sheard \(1999\)](#) report that since 1900 mean annual temperature has increased by about 0.3 °C in Indonesia, whilst the overall annual precipitation has decreased by 2–3%. They report a decline in annual rainfall in the southern regions, and an increase in the northern regions.

Spatially, the islands have very steep climate gradients, related to their mountainous terrain and complex coastlines. To account for this, downscaled or fine-scale climate change projections are required. Downscaling to 60 km resolution over Indonesia has been undertaken previously ([Katzfey et al., 2010](#)). Whilst this resolution should be adequate for capturing the broad seasonal migration of the Inter Tropical Convergence Zone, and the associated seasonal cycle in rainfall, it is still inadequate for capturing the detailed seasonal orographic interactions that are required to properly inform adaptation planning processes ([Butler et al., 2014, 2015](#)), such as presented in this special issue ([Butler et al., 2016](#)). In this paper we describe the methodology and provide selected results for climate projections downscaled to 14 km in the islands of Lombok and Sumbawa, Nusa Tenggara Barat (NTB) Province (Fig. 1). A map showing the NTB province in relation to the whole of Indonesia is provided by [Kirono et al. \(2016\)](#). These simulations represent the first time regional climate simulations have been performed at such high resolution over the Indonesia region.

For downscaling to a fine resolution, various methodologies may be used. The earliest method, and still being used, is to use a limited-area model, forced at its lateral boundaries by a host Global Climate Model (GCM). There are a number of reviews of this methodology (e.g. [McGregor, 1997](#); [Wang et al., 2004](#)). Limited-area models inherit large-scale errors that may exist in the host GCM and this can be problematic (e.g. [Pielke and Wilby, 2012](#)). The downscaling methodology adopted for this study proceeds with a variable-resolution GCM, the conformal-cubic atmospheric model (CCAM). A review of current variable-resolution GCMs is given by [McGregor \(2013\)](#).

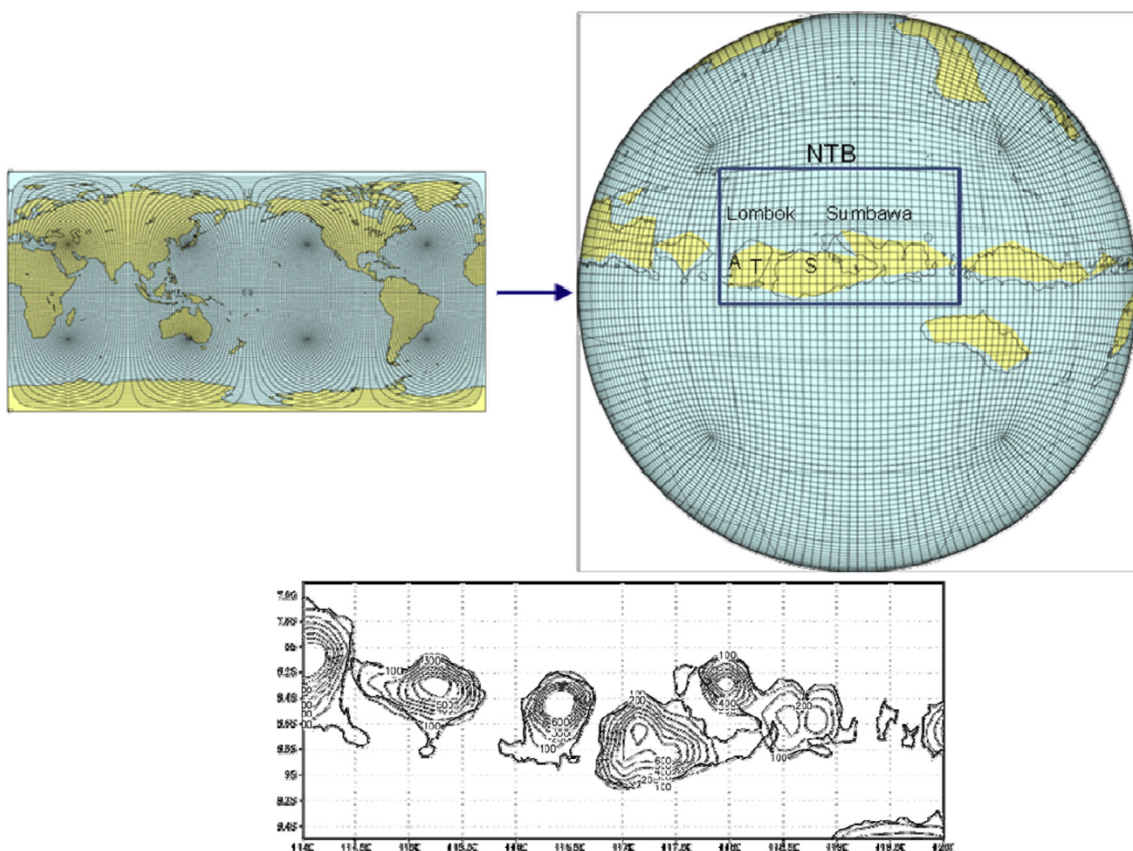


**Fig. 1.** The 200 km global grid (top left), and the 14 km stretched grid (top right) for the eastern Indonesian archipelago, showing NTB, Lombok and Sumbawa. The symbols A, T and S denote respectively the station locations of Ampenan, Terara and Sumbawa. The model orography (m) is also shown (bottom) over a domain that extends somewhat beyond NTB.

Coupled GCMs have coarse resolution, but importantly also possess sea surface temperature (SST) biases; a common bias is excessively cool water (a “cold tongue” bias) over the equatorial Pacific (Zheng et al., 2012), which may distort the ENSO behaviour of the GCM simulations. Any distortion of the ENSO behaviour in host GCMs can have significant impact on the interannual variability of the climate of the study region, as this NTB region is strongly influenced by ENSO variations. Our methodology incorporates corrections of the biases of the present-day forcing SSTs of each host GCM, whereby biases such as the “cold tongue” bias are removed. First, six quasi-uniform simulations at a resolution of 200 km were performed with CCAM, based on GCMs from the Coupled Model Intercomparison Project phase 3 (CMIP3; see Smith and Chandler, 2010) for the period 1971–2100. The 200 km simulations were further downscaled to 14 km over eastern Indonesia for the period 1971–2100. The use of an ensemble of six simulations attempts to capture the uncertainty of the climate projections. The resulting six 14 km simulations provide detailed regional information about climate change and model-to-model variations in simulated climate.

The CCAM downscaling methodology developed for this project has been successfully applied in other CCAM studies to provide ensembles of simulations downscaled from GCMs. The earlier CCAM downscaling project over Indonesia (Katzfey et al., 2010) similarly used bias-corrected SSTs to force a quasi-uniform 200 km global CCAM simulation, which was then further downscaled to 60 km. Those present-day simulations showed temperature improvements compared to the host GCMs and modest rainfall improvements. In a recent large project, six global 60 km quasi-uniform CCAM simulations were performed (Nguyen et al., 2011) driven by bias-corrected SSTs, then further downscaled to 8 km over 7 Pacific Island countries. For another recent large project, six global 50 km quasi-uniform CCAM simulations were performed (Katzfey et al., 2014) driven by bias-corrected SSTs, then further downscaled to 10 km over Vietnam.

The paper is structured into four sections. In Section “CCAM model description and experimental design” the CCAM model and the methodology are described in detail. In Section “Model validation against present day observations” results of the simulations are validated against present-day conditions (1971–2000). Section “Projected future changes for NTB” shows the predicted future changes at 14 km resolution. Finally in Section “Discussion” we discuss some challenges and implications of these results for adaptation planning.

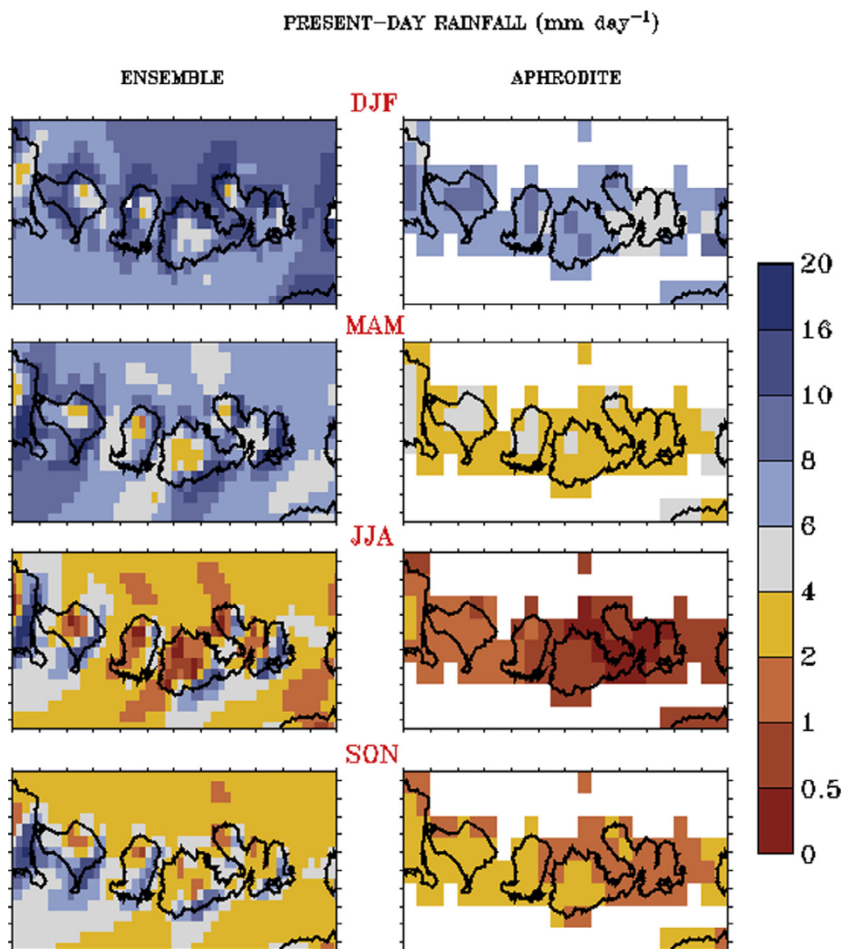


**Fig. 2.** Four seasons (DJF, MAM, JJA, SON) of rainfall (mm/day) for 1971–2000 for the ensemble of 14 km simulations (left) and APHRODITE (right).

## CCAM model description and experimental design

CCAM is a semi-implicit, semi-Lagrangian atmospheric model developed at CSIRO (McGregor, 2005; McGregor and Dix, 2001, 2008); these simulations utilise the hydrostatic primitive equations. CCAM includes a fairly comprehensive set of physical parameterizations. The GFDL parameterizations for long-wave and short-wave radiation (Lacis and Hansen, 1974; Schwarzkopf and Fels, 1991) are employed, with interactive cloud distributions determined by the liquid and ice-water scheme of Rotstayn (1997). The model employs a stability-dependent boundary layer scheme based on Monin–Obukhov similarity theory (McGregor et al., 1993). A canopy scheme is included, as described by Kowalczyk et al. (1994), having six layers for soil temperatures, six layers for soil moisture (solving Richard's equation), and three layers for snow. The cumulus convection scheme uses mass-flux closure, as described by McGregor (2003), and includes downdrafts, entrainment and detrainment. CCAM is well-suited to regional climate modelling due to its variable-resolution global grid. This allows it to be used in a quasi-uniform mode or with a stretched grid for a regional focus, by utilising the Schmidt (1977) transformation.

For this project, CCAM was first set up on a quasi-uniform C48 grid having a resolution of about 200 km over the whole globe (Fig. 1). It was run for 130 years corresponding to 1971–2100, using the Delayed Development or 'Business as Usual' SRES A2 emissions scenario (IPCC AR4 WG1, 2007), driven by (uncorrected) sea-ice and bias-corrected SSTs of a host GCM. To provide an ensemble of results, separate simulations were performed from six host GCMs. A number of previous CCAM simulations have downscaled the reanalyses of the National Centers for Environmental Prediction (NCEP) for 1988–1998, obtaining generally good agreement with present-day climatologies of rainfall over the Asian monsoon region and also with maximum and minimum surface-air temperatures (Nguyen and McGregor, 2009); these simulations were at 60 km resolution and included some validation over Indonesia. It may be noted that the present simulations downscaling from host GCMs provide less certain forcing than from reanalyses, because the latter also include forcing from observed atmospheric fields. We note that it would be possible to utilise forcing from the atmospheric fields of the GCMs, but this would introduce biases from those fields, which are in turn related to the biases of the GCM surface forcings.

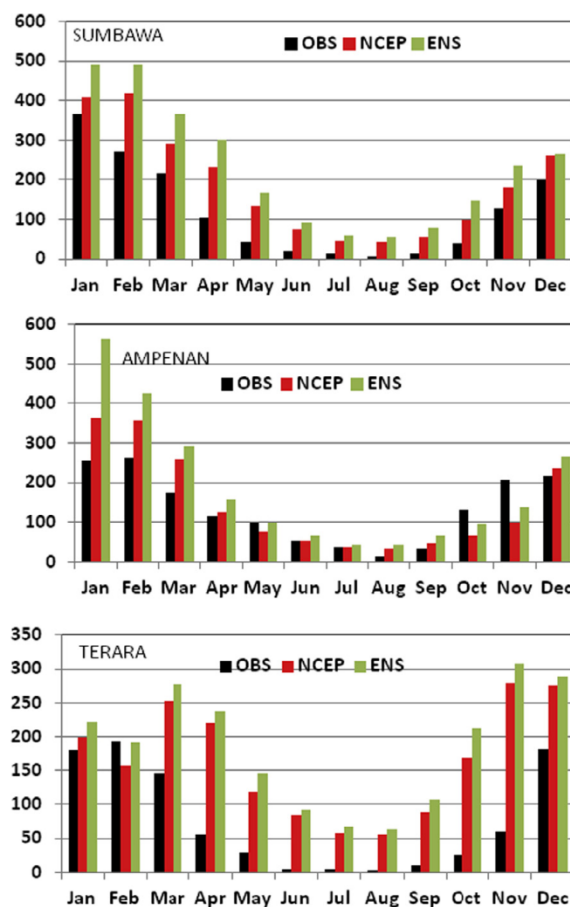


**Fig. 3.** Average (1971–2000) monthly rainfall (mm) for observed (OBS), National Centers for Environmental Prediction (NCEP) and ensemble (ENS) for three stations: Sumbawa, Ampenan (west Lombok) and Terara (central Lombok).

As mentioned above, the host GCMs have significant biases in their SSTs (Zheng et al., 2012). As an example, for present-day conditions the Mk3.5 GCM has an excessively cold equatorial tongue in both January and July of up to 4 °C; in January, there are warm biases of up to 2.5 °C around Indonesia, New Zealand and southwest of Australia; biases of the order of 1 °C exist around Australia in July. Accordingly, average monthly biases are calculated for the SSTs of each GCM corresponding to 1971–2000; these monthly biases are subtracted from the SSTs to provide corrected SSTs throughout each corresponding simulation.

Using CCAM, the 200 km resolution CCAM quasi-uniform global simulations were further downscaled to 14 km resolution for the eastern Indonesian archipelago (Fig. 1). The fine resolution simulations utilised a C48 grid with a Schmidt (1977) stretching factor of 16.7 to provide fairly uniform 14 km resolution from 115–122E. To provide consistency with the 200 km CCAM simulations, a digital filter (Thatcher and McGregor, 2009) was applied every 6 h to replace selected broad-scale (with length scale radius about 15°) atmospheric fields of CCAM with the corresponding broad-scale fields of the 200 km CCAM simulation. In this way the atmospheric behaviour at larger length scales is determined by the 200 km resolution simulations, while the behaviour at small length scales is determined by the 14 km resolution simulation. Those fields are Mean Sea Level (MSL) pressure, moisture, temperature and the wind components above 900 hPa. The CCAM results are compared with observed rainfall, maximum and minimum temperatures.

#### Selected host GCMs

At the time of performing this study, a number of suitable coupled GCMs were available from the Coupled Model Inter-comparison Project (CMIP3; see Smith and Chandler, 2010). From the available emissions scenarios, we chose to use A2 emissions because observed emissions were approximately following A2, and indications were that this will continue to be the most likely scenario. This was important for the adaptation planning process, which sought to model the impacts

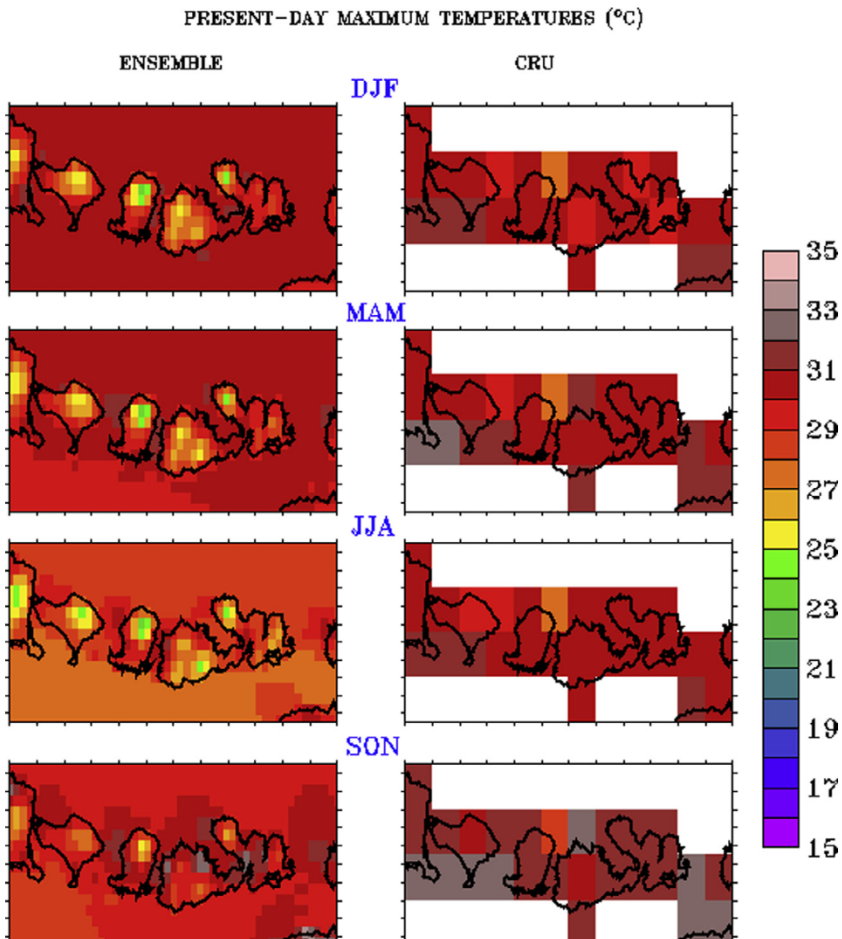


**Fig. 4.** Seasonal plots for average daily maximum surface air temperature (°C) for 1971–2000, for the ensemble-average simulations (left) and the Climate Research Unit (CRU) climatology (right).

on ecosystem goods and services and livelihoods of a ‘Business as Usual’ future ([Skewes et al., 2016](#)). The higher emissions scenario A1FI may be even more likely, but coupled GCMs were not available from CMIP3 for that scenario.

[Smith and Chandler \(2010\)](#) assessed the ability of all CMIP3 GCMs in simulating present-day means and variability over Australia. Based on their study, we chose the following six host GCMs: CSIRO-Mk3.5, GFDL2.0, GFDL2.1, MPI-ECHAM5, HadCM3, Miroc-MedRes. It turned out that the chosen GCMs also show superior present-day ENSO behaviour.

#### Output from the simulations

Six-hourly netcdf output was written on the CCAM 14 km grid for all model fields. The output was also interpolated to a 0.12° latitude-longitude grid covering (113–123E, 5–12S). Monthly-averaged output was written on the 0.12° grid and also on a 0.5° grid covering much of Indonesia (95–140E, 11S–7N). The output written to the latitude-longitude grid includes all surface variables and fluxes, and all model variables on the lowest (40 m) model level.

#### Model validation against present day observations

For validation, we concentrate on results from the ensemble of 14 km simulations. Some results are also provided from simulations downscaling NCEP reanalyses directly to 14 km.

##### Rainfall

Indonesia has a complicated monsoonal behaviour, with several different zones ([Aldrian and Susanto, 2003](#)). Seasonal rainfall is shown in [Fig. 2](#) over an extended NTB domain (114–120E, 7.5S–9.5S) for the present-day period 1971–2000.

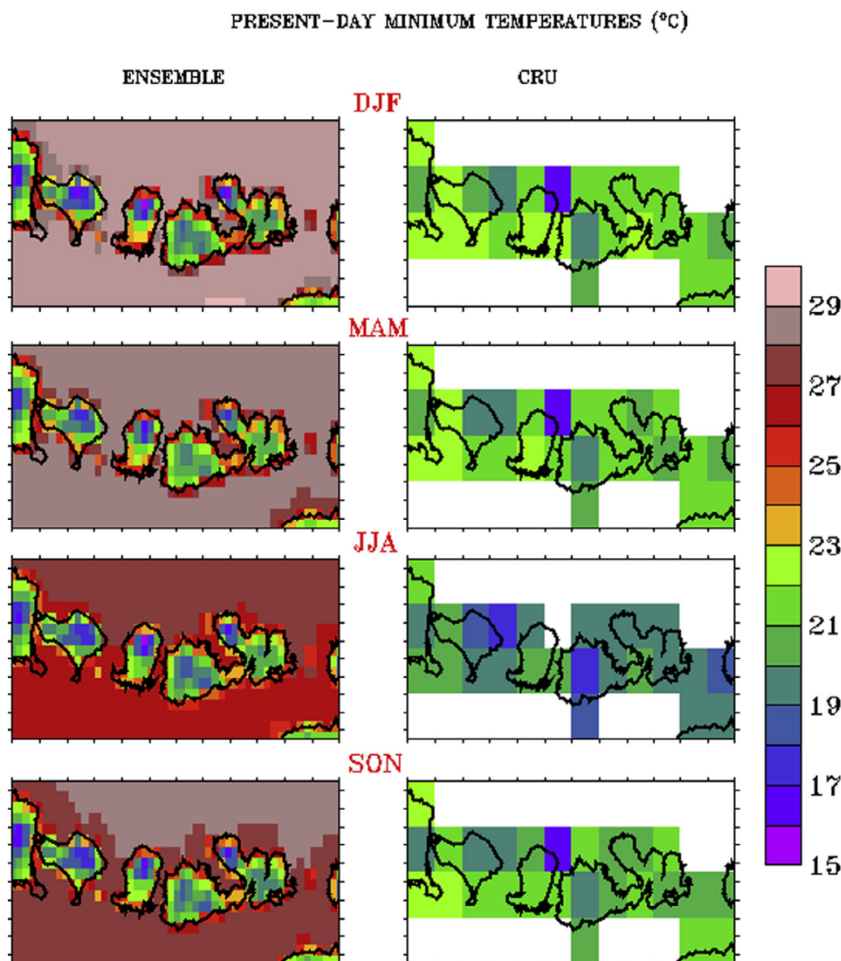


**Fig. 5.** Seasonal plots for average daily minimum surface air temperature (°C) for 1971–2000, for the ensemble-average simulations (left) and the Climate Research Unit (CRU) climatology (right).

The ensemble-average plots may be compared with gridded observational rainfall (on a 0.25° grid) provided by the Asian Precipitation Highly Resolved Observational Data Integration Towards Evaluation of Water Resources project (APHRODITE, [Yatagai et al., 2012](#)).

As can be seen in [Fig. 2](#), the seasonality of the ensemble of simulations generally agrees with the APHRODITE data, for December–January–February (DJF), March–April–May (MAM), June–July–August (JJA), September–October–November (SON). However, rainfall is over-estimated, especially during JJA and SON on the southeast coastlines when the prevailing winds are from the east. It should be noted that observations used by APRHRODITE are rather sparse over Indonesia. Hence it is difficult to validate precipitation in spatial detail over the islands of Lombok and Sumbawa. The present-day rainfall of the individual simulations (not shown) is quite similar to that of the ensemble. This is to be expected because of the great similarity of the present-day monthly-average forcing SSTs of the ensemble members, as a consequence of the bias-correction of their present-day SSTs.

For detail over the islands, one should compare against station observations as in [Fig. 3](#), which shows monthly rainfall (mm/month) for three stations over NTB: Ampenan in west Lombok, Terara in central Lombok, and Sumbawa. The plots show observed rainfall, and also ensemble rainfall. Rainfall is also shown from a 14 km simulation downscaling NCEP reanalyses. The plots show that observed NTB rainfall is generally largest in December–March with the rainfall above 250 mm/month for Ampenan and Sumbawa, whilst in July–September there is low rainfall at under 20 mm/month. Over NTB the modelled rainfall is somewhat excessive, especially for the Terara station, although the seasonality is quite satisfactory. Most of the three stations show correct seasonality of the modelled rainfall.

It may also be noted that the monthly rainfall totals for the CCAM-ENS downscalings are generally higher than those obtained through the CCAM-NCEP downscalings. The nudged NCEP runs constrain the model temperature field to be less in balance with the convection scheme. In the ENS runs, the temperature and moisture field will come into better balance with the convection scheme, which evidently results in slightly more rainfall.

#### *Maximum and minimum surface air temperatures*

A comparison between observed and simulated average daily maximum surface air temperatures for each of the four seasons is provided in [Fig. 4](#). In this figure the ensemble values are compared against the Climate Research Unit (CRU) data set, which has a fairly coarse resolution of 0.5° latitude–longitude. The values agree quite well, although the simulated values are

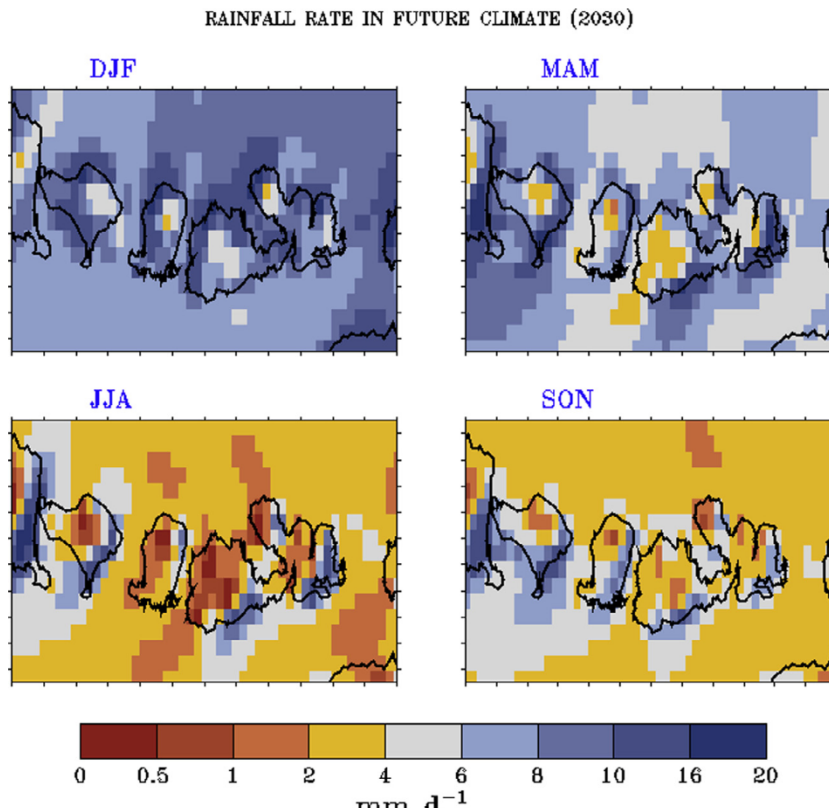


**Fig. 6.** Simulated ensemble rainfall for 2060 (2051–2070), for the four seasons.

1–2 °C cooler than CRU data. Over mountainous areas, the maximum temperatures are rather cooler than the CRU data, but this is reasonable and desirable as the CRU data do not include mountain values. Fig. 5 provides a similar comparison for the simulated average daily minimum surface air temperatures, also for the four seasons. Again the values agree quite well for all seasons, with the simulated fields showing extra detail over coastal and mountainous areas. The main differences from CRU are in DJF and MAM when southern Lombok seems to have warmer simulated minimum temperatures.

## **Projected future changes for NTB**

This Section discusses the downscaled simulations of future climate, concentrating on the ensemble-average results. Some future rainfall information is also provided from the individual model runs to illustrate the range of changes and uncertainty associated with model-to-model variations. Results from two future periods are shown, centred on 2030 (2021–2040) and 2060 (2051–2070). We first show the 2060 period as the changes are more substantial.

### *Simulated rainfall changes by 2060*

The spatial patterns of simulated ensemble-average rainfall for 2060 are shown in Fig. 6. The future ensemble spatial rainfall patterns are very similar to present-day spatial rainfall patterns, so it is not easy to see the differences. To elucidate the patterns of change, Fig. 7 shows the percentage rainfall changes for the ensemble-average of the simulations. For DJF there are small increases above 5% in rainfall on eastern Lombok and south-eastern Sumbawa, with similar decreases elsewhere. For MAM there are general decreases of around 10% with a small area of increase in northeast Lombok. For JJA there is mostly little change from the present. Likewise in SON the rainfall is mostly unchanged except for some reductions in northern Lombok and eastern Sumbawa.

## *Variation among ensemble members of simulated rainfall changes for 2060*

Here we provide an assessment of the variation in rainfall changes among the ensemble members. Fig. 8 shows the ensemble-highest percentage rainfall change at each grid point. Fig. 9 similarly shows the ensemble-lowest rainfall change at each grid point. These figures indicate that there exists a large variation in response among the ensemble members, related to the variation of future SST patterns among the host GCMs. The outlier “wet” scenario models of Fig. 8 are GFDL2.0

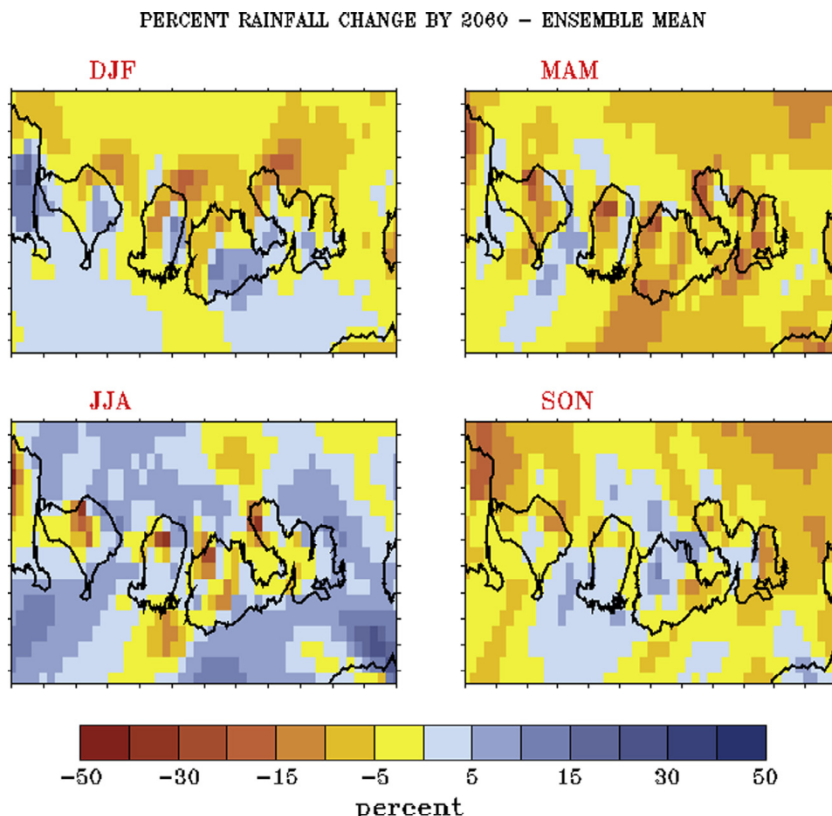


**Fig. 7.** Simulated ensemble-average percentage rainfall change (%) for 2060 (2051–2070), for the four seasons.

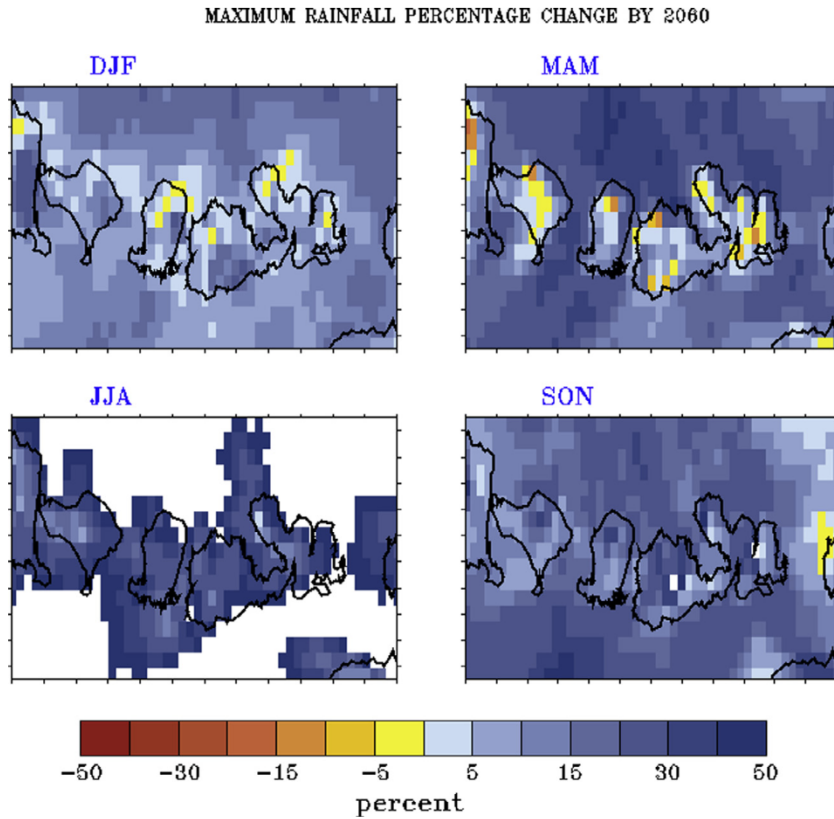


**Fig. 8.** Simulated ensemble-highest percentage rainfall change (%) at each grid point by 2060, for the four seasons.

and Mk3.5 for DJF and MIROC for JJA. The outlier “dry” scenario models of Fig. 9 are UKMO for DJF and Mk3.5 for the other seasons. As with the rainfall changes of the host GCMs there is much variation in the simulated rainfall changes over this region. In forming an ensemble average, our approach is to advocate usage of the simple ensemble-average changes, rather than attempt to exclude outlier models. This is because our initial choice of host GCMs considered them all to provide feasible simulations of future SST patterns; taking the ensemble average will act to cancel biases in the responses of the individual GCMs. Since all the projections are credible and equally plausible, adaptation strategies should really take into account that there is uncertainty in the range of projected rainfall futures – that is, preparations should be made for a significantly drier future, and for a significantly wetter future.

#### *Simulated rainfall changes by 2030*

The spatial patterns of future ensemble-average rainfall centred on 2030 are again mostly very similar to the modelled present-day patterns of rainfall. In Fig. 10 we show the percentage change of the 2030 rainfall compared to present-day. The percentage changes are quite similar to those for 2060 shown in Fig. 7, but the changes are mostly smaller in magnitude. The largest differences between the figures are seen over ocean areas in JJA, with some 5% rainfall increases for 2060 replaced by 5% rainfall decreases for 2030. The signs of change over land areas are mostly the same as for Fig. 7, but with smaller magnitudes. It may be noted that over the land areas some locations show an increase of a few percent for 2060 in JJA and SON, but show a decrease of a few percent in 2030.

#### *Simulated rainfall changes for Ampenan station*

It is informative to show monthly rainfall and its changes for a selected Lombok station, Ampenan. Fig. 11 shows observed rainfall and ensemble-average model changes for 2030, 2060 and 2090. As noted earlier, future rainfall patterns are very similar to present-day modelled patterns and this is also apparent in Fig. 11. January seems to show a small decrease with time, whilst February displays a smaller increase with time.

The individual rainfall amounts for 2060 of each of the ensemble members are displayed in Fig. 12. The present-day ensemble rainfall, EN1990, is also included. Note that each of the individual simulations has similar present-day rainfall to EN1990, with largest variations in January, February and December. It can be seen that for most months, most of the

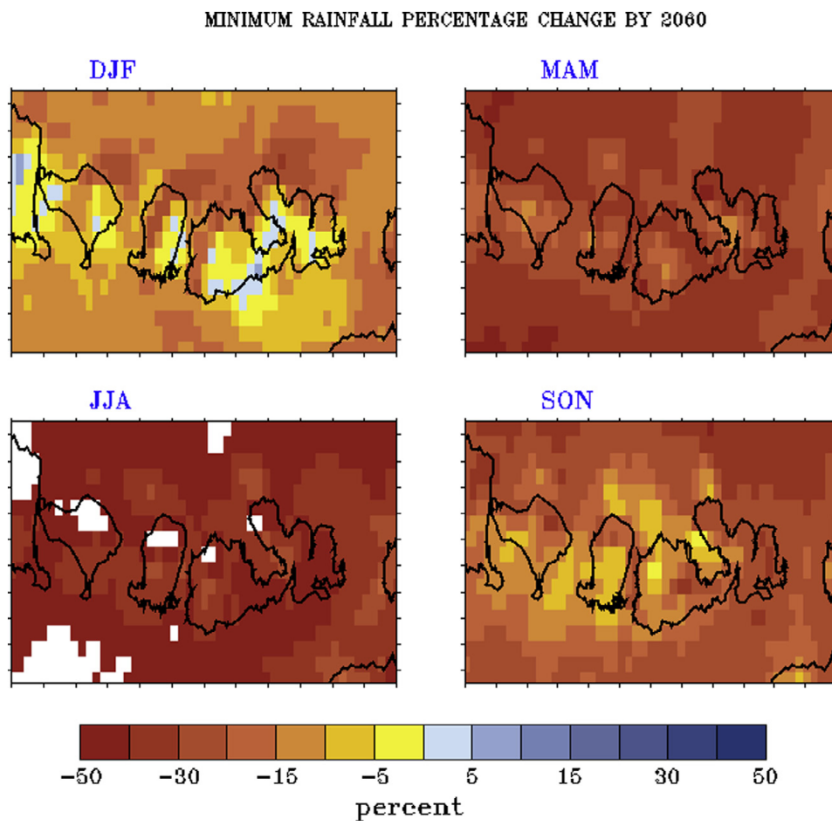


**Fig. 9.** Simulated ensemble-lowest percentage rainfall change (%) at each grid point by 2060, for the four seasons.

simulations show reduction at Ampenan, with GFDL2.0 being driest. The Mk3.5 simulation is the main outlier in this regards, indicating wetter months for December, January and February.

#### Simulated temperature changes by 2030 and 2060

As expected, the surface air temperatures will increase over the NTB region essentially in accord with the six host GCMs. To provide an indication of the behaviour, we show in Fig. 13 the changes in annual-average surface air temperatures from the ensemble average of the simulations. By 2030 the average temperatures will increase by about 1°. By 2060 the temperature increases range from 1.6° to 2°.

#### Discussion

This paper has described the methodology used to dynamically downscale six of the GCM simulations conducted for the CMIP3 SRES A2 emission scenario, historical and future. The variable-resolution CCAM atmospheric model has been used first at a resolution of 200 km for 130-year simulations; those simulations were then downscaled to a fine resolution of 14 km over NTB. The SSTs from the host GCMs were corrected for their present-day biases. The simulations were validated against gridded CRU and APHRODITE data and against observed NTB station data. Rainfall seasonality was generally well captured, though rainfall was over-estimated on the southeast coasts of Lombok and Sumbawa especially during the dry seasons (June–November). The maximum and minimum surface air temperatures were generally in accord with the observational dataset of CRU.

The forcing SSTs of the six GCMs provide a wide range of rainfall responses over the NTB region for the ‘Business as Usual’ scenario. Since all the projections are credible and equally plausible, adaptation strategies should take into account that there is uncertainty in the range of projected rainfall futures, and thus planners should allow for a range of different plausible rainfall futures over NTB. It should also be noted that we did not model the SRES A1FI scenario because the data were unavailable, and this scenario may yield more extreme changes.

The future climatology of the ensemble of simulations was shown for 2030 and 2060. It is noted that the spatial patterns of seasonal rainfall for 2030 and 2060 are extremely similar to the present day. For 2060, the rainfall changes range from zero up to 5–10%, with some increases in DJF and decreases in MAM. The model-to-model percentage changes in rainfall are large,

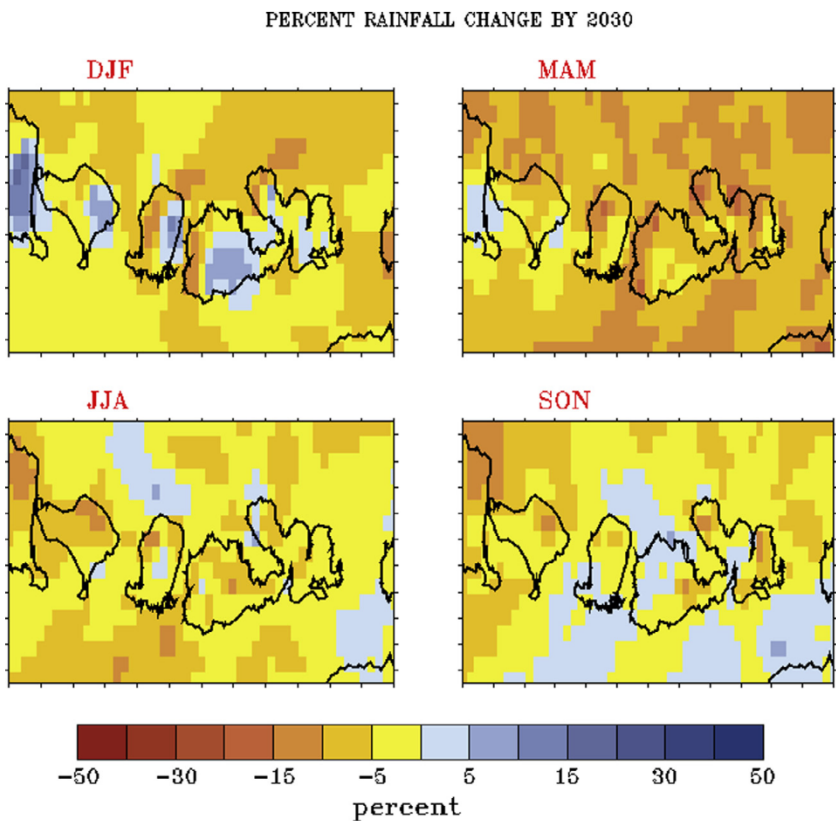


**Fig. 10.** Simulated ensemble percentage rainfall change (%) by 2030 (2021–2040), for the four seasons.

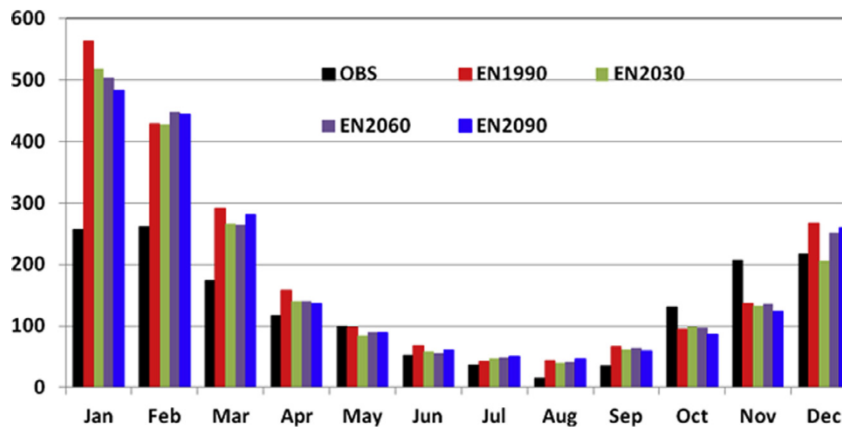


**Fig. 11.** Observed and simulated monthly rainfall at Ampenan: observed (OBS), present-day ensemble-average (EN1990), and ensemble-average rainfall centred on 2030, 2060 and 2090.

but when averaged they produce small changes as large differences may be cancelled. The changes for 2030 are similar to those of 2060, but have smaller magnitude. These fine-scale simulations generally indicate a reduction in rainfall over eastern Indonesia in DJF and MAM, but some regions show increases in DJF.

We note that the six simulations provide regional information about climate change to assist in decision making. The fine 14 km scale allows the incorporation of realistic topographic and land use characteristics, thus providing projections with improved detail. The fine resolution illustrates steep climate gradients across short distances due to the orographic effects of Mount Rinjani and Mount Tambora. For example, rainfall in DJF in north Lombok in 2060 may change by -5% to -20%, whereas in central Lombok it may change by -5% to +10%. This level of detail is clearly important for adaptation planning.

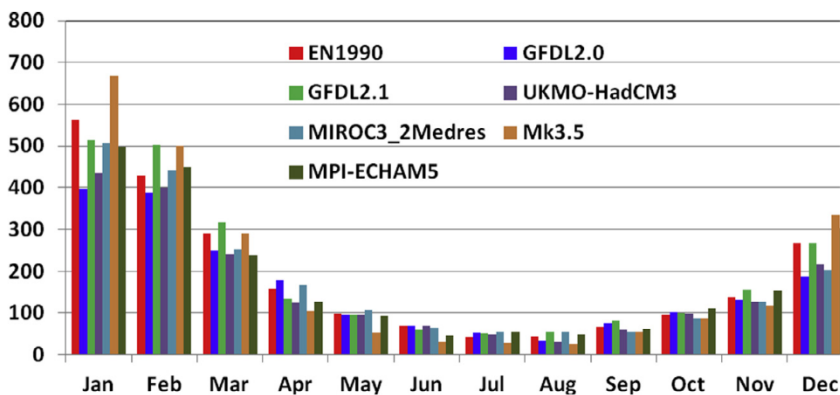


**Fig. 12.** Simulated monthly rainfall for 2060 for Ampenan, for the six downscaled simulations: GFDL2.1, GFDL2.0, UKMO-HadCM3, MIROC3-2, Mk3.5, MPI-ECHAM5. Also shown is the present-day ensemble-average rainfall, EN1990.

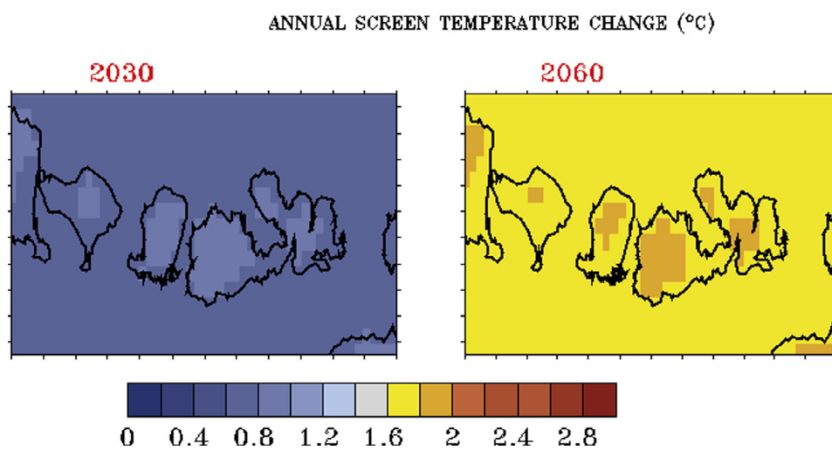


**Fig. 13.** Change of annual-average surface air temperature (from present-day) derived from the ensemble-average by 2030 (2021–2040) and by 2060 (2051–2070), relative to 1971–2000.

because such differences in projections have implications for the design of appropriate strategies, as discussed elsewhere in this special issue (Butler et al., 2016). Vulnerabilities to climate change include changes in species distribution, impacts on agriculture and infrastructure, and also application of these scenarios for engineering purposes (Kirono et al., 2016).

There are a number of caveats that apply to the simulated projections. First, there is some uncertainty regarding the rate of increase of greenhouse gases emissions (IPCC AR4 WG1, 2007). The individual GCMs also produce a range of changes of SST patterns due to their different methods of modelling the many contributing climate processes; taking an ensemble average helps to cancel out the individual uncertainties in those SST changes, and thus in their associated rainfall changes. By producing an ensemble of downscaled simulations, one can also obtain an estimate of the uncertainty of the climate projections. We also removed the average monthly SST biases in our simulations, which permits an improved estimate of present-day climatology. We note that it is especially difficult to capture fully the range of rainfall behaviour of the tropical Indonesian region, largely related to the challenge of modelling cumulus precipitation for this region with its complex coastline and many small islands. However, by concentrating on the rainfall changes rather than absolute values, the present-day biases have less importance.

We note that it is beyond the scope of this paper to produce analyses of extreme events such as intense rainfall events or droughts. However, it would be possible to perform such analyses on the six-hourly output provided by these simulations. In this context it should be noted that when averaging the simulations to form an ensemble, information about extreme events is lost in the process of calculation. Averaging gives the climatological signal, but not the changes in extreme events, which can be very important for impact assessments.

A large amount of model output has been generated. These data can be applied to drive other tools, such as crop, storm surge and hydrological models in order to inform adaptation planning. It may be noted that a previous study, the Lombok Vulnerability Assessment (Ministry of Environment, 2009), was concerned that the SST output over the Pacific Ocean from a single Meteorological Research Institute (MRI) GCM was indicating that the ENSO frequency may have a 2–3 year cycle

during 2001–2030, rather than the current 5–7 year cycle. Our simulations do include ENSO cycles and it may be interesting and worthwhile to carry out a comprehensive analysis using our ensemble of simulations. However, it should be noted that our simulations contain the same ENSO cycles as the host GCMs, and it is now known that CMIP5 GCMs do not consistently indicate a change in ENSO magnitude or frequency (Taschetto et al., 2014).

## Acknowledgements

The research was funded by the Australian Department of Foreign Affairs and Trade (DFAT) as part of the DFAT-CSIRO Research for Development Alliance. Helpful comments on the manuscript were provided by Dr Ramasamy Suppiah and Dr James Butler (CSIRO) and Dr Milind Mujumdar (Indian Institute of Tropical Meteorology) and by two anonymous reviewers.

## References

- Aldrian, E., Susanto, R.D., 2003. Identification of three dominant rainfall regions within Indonesia and their relationship to sea surface temperature. *Int. J. Climatol.* 23, 1435–1452.
- Butler, J.R.A., Suadnya, W., Puspadi, K., Sutaryono, Y., Wise, R.M., Skewes, T.D., Kirono, D., Bohensky, E.L., Handayani, T., Habibi, P., Kisman, M., Suharto, I., Hanartani, , Supartarningsih, S., Ripaldi, A., Fachry, A., Yanuartati, Y., Abbas, G., Duggan, K., Ash, A., 2014. Framing the application of adaptation pathways for rural livelihoods and global change in Eastern Indonesian islands. *Global Environ. Change* 28, 368–382.
- Butler, J.R.A., Wise, R.M., Skewes, T.D., Bohensky, E.L., Peterson, N., Suadnya, W., Yanuartati, Y., Handayani, T., Habibi, P., Puspadi, K., Bou, N., Vaghelo, D., Rochester, W., 2015. Integrating top-down and bottom-up adaptation planning: a structured learning approach. *Coastal Manage.* 43, 346–364.
- Butler, J.R.A., Bohensky, E.L., Darbas, T., Kirono, D., Wise, R.M., Sutaryono, Y., 2016. Building capacity for adaptation pathways in eastern Indonesian islands: synthesis and lessons learned. *Clim. Risk Manage.* 12, A1–A10.
- Hulme, M., Sheard, N., 1999. *Climate Change Scenarios for Indonesia*. Climatic Research Unit, Norwich, UK, 6 pp.
- IPCC AR4 WG1, 2007, Contribution of Working Group I to the Fourth Assessment Report of the Intergovernmental Panel on Climate Change. In: Solomon, S., Qin, D., Manning, M., Chen, Z., Marquis, M., Averyt, K.B., Tignor, M., Miller, H.L. (Eds.), *Climate Change 2007: The Physical Science Basis*, Cambridge University Press, ISBN 978-0-521-88009-1 (pb: 978-0-521-70596-7).
- Katzfey, J., McGregor, J.L., Nguyen, K., Thatcher, M., 2010. Regional climate change projection development and interpretation for Indonesia. CSIRO Marine and Atmospheric Research Final Report for AusAID, 36 pp.
- Katzfey, J.J., McGregor, J.L., Suppiah, R. (Eds.), 2014. High-resolution climate projections for Vietnam: Technical Report. CSIRO, Australia, 266 pp.
- Kirono, D., Butler, J.R.A., McGregor, J., Ripaldi, A., Katzfey, J., Nguyen, K., 2016. Historical and future seasonal rainfall variability in Nusa Tenggara Barat Province, Indonesia: implications for the agriculture and water sectors. *Clim. Risk Manage.* 12, 45–58.
- Kowalczyk, E.A., Garrett, J.R., Krumml, P.B., 1994. Implementation of a soil-canopy scheme into the CSIRO GCM – regional aspects of the model response. CSIRO Division of Atmospheric Research Technical Paper No. 32.
- Lacis, A., Hansen, J., 1974. A parameterization for the absorption of solar radiation in the Earth's atmosphere. *J. Atmos. Sci.* 31, 118–133.
- McGregor, J.L., 1997. Regional climate modelling. *Meteorol. Atmos. Phys.* 63, 105–117.
- McGregor, J.L., 2003. A new convection scheme using a simple closure. *BMRC Res. Rep.* 93, 33–36.
- McGregor, J.L., 2005. CCAM: geometric aspects and dynamical formulation [electronic publication]. CSIRO Atmospheric Research Technical Paper No. 70.
- McGregor, J.L., 2013. Recent developments in variable-resolution global climate modelling. *Clim. Change* 119. <http://dx.doi.org/10.1007/s10584-013-0866-5>.
- McGregor, J.L., Dix, M.R., 2001. The CSIRO conformal-cubic atmospheric GCM. In: Hodnett, P.F. (Ed.), *IUTAM Symposium on Advances in Mathematical Modelling of Atmosphere and Ocean Dynamics*. Kluwer, Dordrecht, pp. 197–202.
- McGregor, J.L., Dix, M.R., 2008. An updated description of the conformal-cubic atmospheric model. In: Hamilton, K., Ohfuchi, W. (Eds.), *High Resolution Simulation of the Atmosphere and Ocean*. Springer, pp. 51–76.
- McGregor, J.L., Gordon, H.B., Watterson, I.G., Dix, M.R., Rotstayn, L.D., 1993. The CSIRO 9-level atmospheric general circulation model. CSIRO Division of Atmospheric Research Technical Paper No. 26.
- Ministry of Environment, 2009. Risk and Adaptation Assessment to Climate Change in Lombok Island West Nusa Tenggara Province. Indonesia Ministry of the Environment (Kementerian Lingkungan Hidup), GIZ, WWF, Jakarta, Indonesia.
- Nguyen, K.C., McGregor, J.L., 2009. Modelling the Asian summer monsoon using CCAM. *Clim. Dyn.* 32, 219–236.
- Nguyen, K.C., Katzfey, J.J., McGregor, J.L., 2011. Global 60 km simulations with CCAM: evaluation over the tropics. *Clim. Dyn.* <http://dx.doi.org/10.1007/s00382-011-1197-8>.
- Pielke, R.A., Wilby, R.L., 2012. Regional climate downscaling: What's the point? *EOS* 93, 52–53.
- Rotstayn, L.D., 1997. A physically based scheme for the treatment of stratiform clouds and precipitation in large-scale models. I: description and evaluation of the microphysical processes. *Q. J. R. Meteorol. Soc.* 123, 1227–1282.
- Schmidt, F., 1977. Variable fine mesh in spectral global model. *Beitr. Phys. Atmos.* 50, 211–217.
- Schwarzkopf, M.D., Fels, S.B., 1991. The simplified exchange method revisited: an accurate, rapid method for computation of infrared cooling rates and fluxes. *J. Geophys. Res.* 96, 9075–9096.
- Skewes, T.D., Hunter, C.M., Butler, J.R.A., Lyne, V.D., Suadnya, W., Wise, R.M., 2016. The asset drivers well-being interaction matrix (ADWIM): a participatory tool for estimating future impacts on ecosystem services and livelihoods. *Clim. Risk Manage.* 12, 69–82.
- Smith, I., Chandler, E., 2010. Refining rainfall projections for the Murray darling basin of south-east Australia – the effect of sampling model results based on performance. *Clim. Change*. <http://dx.doi.org/10.1007/s10584-009-9757-1>.
- Taschetto, A.S., Sen Gupta, A., Jourdain, N.C., Santoso, A., Ummenhofer, C.C., England, M.H., 2014. Cold tongue and warm pool ENSO events in CMIP5: mean state and future projections. *J. Clim.* 27, 2861–2885.
- Thatcher, M., McGregor, J.L., 2009. Using a scale-selective filter for dynamical downscaling with the conformal cubic atmospheric model. *Mon. Weather Rev.* 137, 1742–1752.
- Wang, Y., Leung, L.R., McGregor, J.L., Lee, D.-K., Wang, W.-C., Ding, Y., Kimura, F., 2004. Regional climate modelling: progress, challenges, prospects. *J. Meteorol. Soc. Jpn.* 82, 1599–1628.
- Yatagai, A., Kamiguchi, K., Arakawa, O., Hamada, H., Yasutomi, N., Kitoh, A., 2012. APHRODITE: constructing a long-term daily gridded precipitation dataset for Asia based on a dense network of rain gauges. *Bull. Am. Meteorol. Soc.*, 1401–1415
- Zheng, Y., Lin, J.-L., Shinoda, T., 2012. The equatorial Pacific cold tongue simulated by IPCC AR4 coupled GCMs: upper ocean heat budget and feedback analysis. *J. Geophys. Res.* 117, C05024. <http://dx.doi.org/10.1029/2011JC007746>.